RSC Advances

PAPER

View Article Online
View Journal | View Issue

Cite this: *RSC Adv.*, 2015, **5**, 24299

Alkali and alkaline-earth metal complexes with tetraoxa[8]circulene sheet: a computational study by DFT and QTAIM methods†

Nataliya N. Karaush,[a] Gleb V. Baryshnikov*[a] and Boris F. Minaev[ab]

Received 4th November 2014
Accepted 11th February 2015

DOI: 10.1039/c4ra13806f

www.rsc.org/advances

A series of alkali and alkaline-earth metal ion complexes with the tetraoxa[8]circulene sheet which possess single- and double-decker structure has been designed and studied by the DFT computational method. Bader's topological analysis of the electron density distribution function has been also performed for the studied complexes with the aim to determine their peculiar electronic features. The obtained computational results indicate the definite selectivity in respect to complexation of the s-block metal ions with the tetraoxa[8]circulene-formed nanopores of various sizes. The coordination bonds of the s-block metal centers with the neighbouring oxygen atoms in the studied complexes possess predominantly ionic nature and can be interpreted as low-covalence closed-shell interactions. The total complexation energy for the studied systems has been estimated to be in a wide range of 9–60 kcal mol^{-1} which indicates their different stability depending on the nanopore size and metal ion radii. For these reasons the synthesis of the tetraoxa[8]circulene sheets is an important task because of their potential applications as biomimetic-type nanopores representing synthetic ionic channels.

Introduction

Great progress in molecular electronics and materials science areas inevitably led scientists to development of novel molecular electronics devices (molecular conductors, diodes, magnets) and to design and synthesis of novel coordination polymers, sorbents, and ceramics for separation or concentration of substances. Self-assembly by supramolecular coordination on surfaces provided a useful approach for the bottom-up fabrication of two-dimensional (2D) nanostructures. Currently, most of the synthesized metal complexes represent compounds with organic ligands. Moreover the ligands structure can be easily modified by various functional groups, as well as by changing the composition of those ligand parts which are not directly involved into interaction with the central atom. Particularly, the linking of the monodentate ligands can produce bi-, three- and polydentate ligands with unique properties, such as crown ethers,[1,2] porphyrins,[3] phthalocyanines[4] and others.[5]

The first representative of the crown ether class, dibenzo-18-crown-6 (Fig. 1, **a**), was synthesized by C. J. Pedersen[1a,b] as a by-product of the cyclic condensation of pyrocatechol with

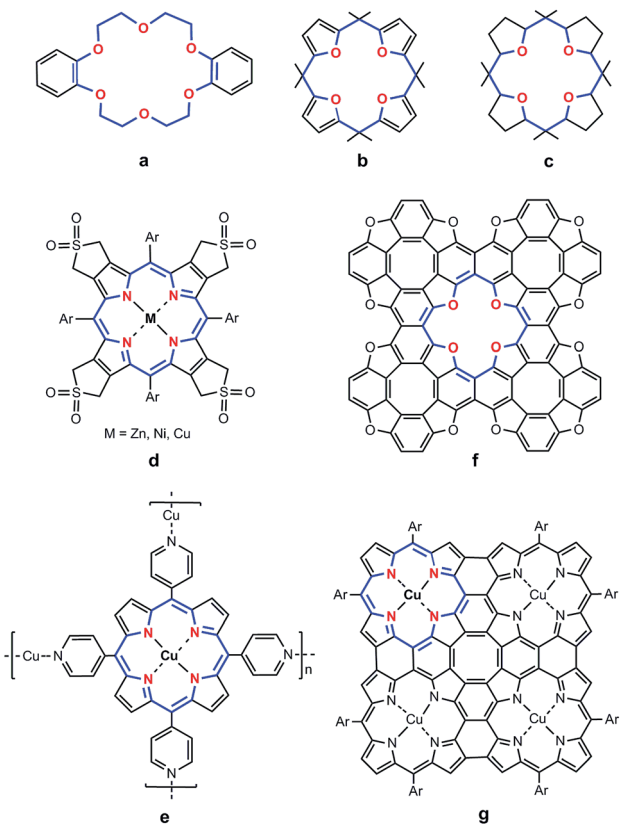

Fig. 1 Some examples of the well known crown ethers **a**–**c** and of the recently synthesized reactive building-blocks containing porphyrin (**d**, **e** and **g**) and tetraoxa[8]circulene (**f**) cores.

[a]*Bohdan Khmelnytsky National University, Cherkasy, 18031, Ukraine. E-mail: glebchem@rambler.ru; bfmin@rambler.ru*

[b]*Tomsk State University, Tomsk, 634050, Russian Federation*

† Electronic supplementary information (ESI) available: Optimized structure and corresponding Cartesian coordinates for the complexes **1**–**7**. See DOI: 10.1039/c4ra13806f

dichlorodiethyl ether in the 2 : 2 ratio. C. J. Pedersen also established that certain polyether macrocycles can bind alkali and alkaline-earth cations,[1c–f] for which he was awarded the Nobel Prize in 1987. This discovery rises a great interest to the "crown ether field". Subsequently, a large number of other novel cation binders were synthesized, including macrocyclic polyether sulfides derivatives.[1e,f]

Compounds, similar to crown ethers (Fig. 1, **b** and **c**), were obtained by Chastrette *et al.*[6] *via* the linear condensation of furan and acetone. Soon after, Y. Kobuke *et al.*[7] have received a series of similar cyclic polyesters containing tetrahydrofuran fragments by the linear oligomers closure into the whole macrocycle. It was found, that these heterocyclic crown ethers demonstrate the ability to extract and transport alkali metal ions through the liquid membrane.[7]

Nowadays, a great attention is attracted to the assembly of surface-supported metaloorganic coordination compounds.[8] As an example, the several transition metal ions (Zn^{2+}, Ni^{2+}, Cu^{2+}) complexes of tetra-*b*″-sulfoleno-*meso*-arylporphyrin (Fig. 1, **d**) were used as the universal reactive building blocks, allowing the construction of more complicated covalent assemblies by the porphyrin-LEGO® approach.[8b,c] Another example of the metal–organic coordination networks synthesis is the formation of copper complexes with 5,10,15,20-tetra(4-pyridyl)porphyrin (2HTPyP, Fig. 1, **e**) assembled on Au(111) surface[8d] which produces a mixed-valence coordination network with alternating Cu(0) and Cu(II) centers.

The rapid development of circulene‡[9,10] and circulene-like[11a,b] chemistry during last few years led to a number of theoretical predictions of the new oligomers and polymers based on the tetraoxa[8]circulene (TOC) unit called also the TOC sheets.[10f,g] Supramolecular coordination self-assembled structures based on TOC units have been predicted recently by DFT simulation.[10g,h] These theoretically invented organic 2D polymers seem to be promising objects because of their unique optical, magnetic and structural peculiarities which provide possible applications in electronics, catalysis, solid sensors, and especially in separation and storage of small species, in the form of ionic sieves.

In general, the unique structure of the TOC sheets (Fig. 1, **f**) allows to use them in order to form selectively the metal ion complexes by capture the metal ions which size correlates with the size of the macrocycle cavity. Thus, such TOC sheets seem to be the possible analogues for biological channels which play a key role in transport phenomena[11c] of the s-block metal cations through the cell membranes. Recently, Kang *et al.* have designed computationally the similar biomimetic graphene-based nanopores containing oxygen atoms.[11d] The synthesis of the TOC-sheet N-analogues was experimentally realized by Nakamura *et al.*[12] resulting in the free base and Cu(II) complex (Fig. 1, **g**) of a square porphyrin sheet with a planar cyclooctatetraene core. We should note that recently much attention has also paid to the synthesis of functionalized sandwich-type (double-decker) metal complexes containing macrocyclic ligands. For instance, the phthalocyanine double-decker complexes have been recently studied in details.[13]

Following this line we have considered in the present paper a possibility of the alkali and alkaline-earth ions binding by the TOC-tetramer (Fig. 2 and 3) on the basis of the DFT modelling including the complete analysis of the electron density distribution function by the Bader's algorithm[14] with the aim to describe the coordination bonds features and to estimate the stability of the designed complexes.

The selective s-block metal complexation with the TOC sheet looks as a promising approach because of its close similarity with the biological ionic channels selectivity[15] which makes actual the synthesis of the predicted TOC sheets.[10f,g]

Method of calculation

The equilibrium geometry parameters of the studied complexes **1**–**7** (Fig. 2 and 3) have been optimized at the density functional theory (DFT[16]) computational level using the Becke–Lee–Yang–Parr three-parametric exchange-correlation functional (B3LYP[16]) and the 6-31G(d)[17a] basis set for the light atoms and the effective core potential Lanl2DZ[17b] basis set for the heavy Ba and Sr atoms. We have also calculated the IR absorption spectra for the studied complexes at the same computational method; the absence of imaginary frequencies in the corresponding IR spectra provides us evidence that the true energy minimum was found.

On the basis of the obtained equilibrium geometries, we have performed the topological analysis of the electron density distribution function $\rho(\mathbf{r})$ at the Bader's level of Quantum Theory of Atoms in Molecules (QTAIM).[14] The energies of the coordination M–O bonds and of other intermolecular contacts (π-stacking interactions in the sandwich complexes **6** and **7**) have been calculated by the Espinosa relationship[18] which is widely used for the energy estimation of the M–O, M–N coordination bonds,[18c,d] different types of hydrogen bonds[18b,e] and van-der-Waals interactions:[18f]

$$E = 0.5v(\mathbf{r}), \quad (1)$$

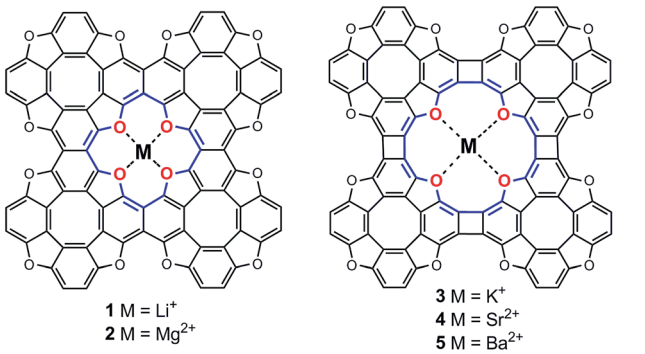

Fig. 2 Structure of the s-block metal (M) complexes with two types of the tetraoxa[8]circulene sheets (the coordination M–O bonds are shown by the dashed lines).

‡ The circulenes family includes the synthesized tetraoxa[8]circulenes, azaoxa[8]circulenes, thio[8]circulenes and some theoretically predicted hetero[8]circulenes (see ref. 9 and 10).

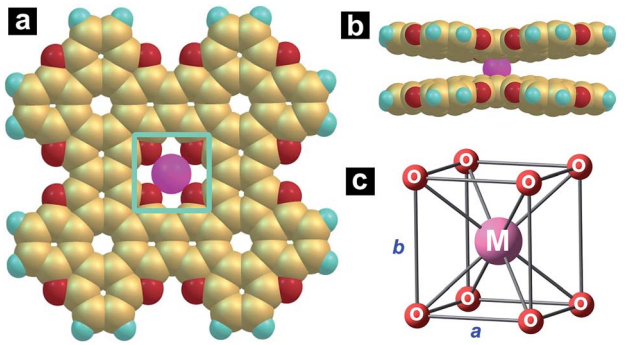

Fig. 3 The optimized structure of the sandwich-type complexes $[M(TOC)_2]^{n+}$ (M = K^+, **6**; Ca^{2+}, **7**): (a) – top view, (b) – side view, (c) – prism-shaped coordination cage consisting of the K^+ or Ca^{2+} ions ($a \neq b$).

where E is the bond energy (au), $\nu(\mathbf{r})$ is the potential energy density (au) at the corresponding (3, −1) critical point.[14] The use of the Bader method makes it possible to describe qualitatively the chemical bond nature based on the signs and values of the electron density Laplacian $\nabla^2\rho(\mathbf{r})$ and of the electron energy density $h_e(\mathbf{r})$ at the corresponding (3, −1) bond critical point in accordance with the following conditions:[14b,19]

(1) $\nabla^2\rho(\mathbf{r}) < 0$, $h_e(\mathbf{r}) < 0$ indicates the shared interactions, *i.e.* weakly polar and nonpolar covalent bonds;

(2) $\nabla^2\rho(\mathbf{r}) > 0$, $h_e(\mathbf{r}) < 0$ indicates the intermediate interactions, which include strong hydrogen bonds and most of the coordination bonds;

(3) $\nabla^2\rho(\mathbf{r}) > 0$, $h_e(\mathbf{r}) > 0$ indicates the closed shell interactions such as weak hydrogen bonds, van-der-Waals interactions, ionic bonds.

The binding energy (BE) of a metal cation to the TOC based ligand is additionally calculated by the following equation in the framework of DFT/B3LYP approach in a gas phase:

$$BE = E(\text{complex}) - [E(M^{n+}) + E(\text{TOC-ligand})].$$

The basis set superposition error (BSSE) was corrected for each binding energy value with the counterpoise method.

Additionally, we have performed the calculation of the dispersion effect upon complexation for the studied **1–7** species by the B3LYP-D approach. These B3LYP-D calculations were performed using the ORCA program package, version 2.8.[20]

All DFT calculations have been performed using the GAUSSIAN09 software.[21] The QTAIM calculations have been carried out using the AIMAll program package.[22]

Results and discussion

1. Structural features and the metal-binding selectivity

As we have shown by DFT optimization the single-decker complexes **1–5** (Fig. 2) and the double-decker sandwich complexes **6** and **7** (Fig. 3) belong to the D_{4h} symmetry point group. Thus, the four M–O bonds in the complexes **1–5** (Fig. 2) and the eight M–O bonds in the **6** and **7** (Fig. 3) species are equivalent in terms of the bond length and electronic criteria for each designed complex (Tables 1 and 2). Thus, the central ion coordination sphere represents the strict planar-square structure for the **1–5** complexes and the proper rectangular prism for the **6** and **7** sandwiches.

The selectivity of complexation of the s-block metals with the TOC sheets can be interpreted in terms of the strict correlation between the size of cation and of the macrocycle cavity in the TOC-tetramer (Fig. 1, **c**) similarly to the crown ethers metal complexes. We have found that the TOC sheet with the 16-crown-4 cavity diameter equals 4.1 Å (distance between the two opposite oxygen atoms) is the most appropriate for inclusion into this cavity of the Li^+ and Mg^{2+} ions (which have the close similar ionic radii 0.59 and 0.57 Å, respectively).[23] Increasing the cavity diameter through introduction of the four-membered rings into the TOC sheet (Fig. 2) makes it possible the inclusion of the larger K^+, Ba^{2+} and Sr^{2+} ions into the 20-crown-4 cavity with ionic radii 137, 135 and 126 pm, respectively (distance between the two opposite oxygen atoms equals 6.0 Å). From the other side, the smaller Li^+, Na^+, Mg^{2+} and Ca^{2+} ions can not be retained in the large 20-crown-4 cavity as well as the bigger K^+, Ba^{2+} and Sr^{2+} ions can not squeeze through the smaller 16-crown-4 cavity due to a strong Coulomb repulsion. However, we do not exclude the possibility of including into the macrocyclic cavity of the cations with smaller ionic radius, but in such way the cation should be displaced from the center of the cavity whereupon it should be attracted to one of the oxygen atoms (similar to some of the crown ether complexes).[24a] If the ions are too large to penetrate a macrocyclic cavity they can sit on the top of the TOC-cavity, which is also similar to some of the crown ethers complexes.[24b,c] However, we have not obtained such stable complexes for the both studied cases. From the other hand we have postulated that the big ions (K^+, Ca^{2+}) are able to form the double-decker sandwich complexes with the two TOC sheet plains. This is one of the few examples of the cubic oxygen coordination around alkali and alkaline-earth metal ions. The structure of these complexes is discussed below in more details.

2. QTAIM analysis of M–O interactions in the single-decker square complexes 1–5

According to the Gauss rule for electrostatic interaction, the binding in ionic systems is achieved due to polarization of the ions in the direction opposite to the charge transfer. In accordance with our quantum-chemical calculations a significant excess of the electron density is observed for the oxygen atoms forming the central crown cavity: the Bader's charges on the oxygen atom for the compounds **1–5** are equal to −1.134*e*, −1.177*e*, −1.121*e*, −1.096*e*, −1.101*e*, respectively. Thus, we can see the monotonous charge decrease in the presented ionic row which is explained by the mutual ion-ligand polarization that in turn determines the corresponding degree of the M–O bonds covalent character.

As one can see from Table 1, the $|\lambda_1/\lambda_3|$ curvature elements ratio for all M–O bonds varies in a short range 0.149–0.189 (*i.e.* $|\lambda_1/\lambda_3| < 1$). This fact indicates the significant exhaustion of the

Table 1 The $\rho(\mathbf{r})$ function curvature element values (λ), their ratios ($|\lambda_1/\lambda_3|$ and $\varepsilon = \lambda_1/\lambda_2 - 1$) at the M–O critical point and some electron density localization parameters (DI – delocalization index, LI – localization index, q – atomic Bader's charge)

Complex	Bond	λ_1, $e \times a_0^{-5}$[a]	λ_2, $e \times a_0^{-5}$	λ_3, $e \times a_0^{-5}$	$\lvert\lambda_1/\lambda_3\rvert$	ε	DI	LI (M)	q
1	$Li^+\cdots O$	-3.26×10^{-2}	-3.15×10^{-2}	0.204	0.160	0.034	0.0511	1.962	0.9265
2	$Mg^{2+}\cdots O$	-5.96×10^{-2}	-5.39×10^{-2}	0.402	0.148	0.105	0.1286	9.932	1.7878
3	$K^+\cdots O$	-9.01×10^{-3}	-8.33×10^{-3}	5.68×10^{-2}	0.159	0.081	0.0545	17.918	0.9601
4	$Sr^{2+}\cdots O$	-1.20×10^{-2}	-1.05×10^{-2}	7.29×10^{-2}	0.165	0.138	0.1002	35.916	1.8484
5	$Ba^{2+}\cdots O$	-1.66×10^{-2}	-1.50×10^{-2}	8.79×10^{-2}	0.189	0.103	0.1307	53.846	1.8546
6	$K^+\cdots O$	-1.19×10^{-2}	-1.13×10^{-2}	7.56×10^{-2}	0.157	0.053	0.0554	17.817	0.9354
7	$Ca^{2+}\cdots O$	-2.15×10^{-2}	-1.99×10^{-2}	0.131	0.164	0.077	0.1166	17.839	1.8078

[a] a_0 is the Bohr radius.

electron density concentration in the interatomic space, which is usually observed for the closed shells interactions.

At the same time the critical points of all M–O bonds satisfy the following condition: $\nabla^2\rho(\mathbf{r}) > 0$ and $h_e(\mathbf{r}) > 0$ ($|\nu(\mathbf{r})| < g(\mathbf{r})$) (Table 2), which additionally allows us to classify the M–O contacts as the closed shells interactions in terms of the Bader theory formalism.[14b,19] Indeed, the very low delocalization index (DI) values for the M–O bonds (Table 1) indicate directly the very low electron density concentration in the intaratomic region between the O and M atoms. By the way, the DI parameter can be directly interpreted as the M–O bond order.[14d] It should be noted, that for the M^{2+}–O bonds (*i.e.* M^{2+} is an alkaline-earth metal ion) the DI values are in the range of 0.1002–0.1307 and are almost twice as much higher than DI values for M^+–O bonds in the alkali metal complexes **1** and **3** (Table 1). As one can see from the Table 1, the calculated DI index directly correlate with the localization indices (LI) values and atomic charge values (q), *viz.* increasing of DI leads to the decreasing of the atomic basin electron population which is defined by the LI and q parameters.

Concerning the stability of the planar square complexes **1–5** it is obvious that the small 16-crown-4 cavity binds the Mg^{2+} or Li^+ cations stronger than the extended 20-crown-4 pore binds the K^+, Ba^{2+}, Sr^{2+} ions. Indeed, the total complexation energy of the Li^+ and Mg^{2+} ions equals to 26.1 and 61.5 kcal mol^{-1}, respectively, which define the great stability of the $[Mg(TOC)]^{2+}$ complex **2**. Higher stability of the $[Mg(TOC)]^{2+}$ complex relative to the complex **1** can be explained by the stronger mutual polarization and electrostatic attraction between the double charged Mg^{2+} ion and oxygen sides. The cation binding energy is much less for the complexes **3–5** (Table 2) due to a big size of the 20-crown-4 cavity which is incompletely compensated by the cation size upon the complexation.

An important criterion of the M–O bonds stability is an ellipticity parameter (ε),[14c] which is easily calculated as the ratio between the $\rho(\mathbf{r})$ curvature elements ($\lambda_1/\lambda_2 - 1$) at the M–O bond critical point. As pointed out by Bader, the cyclic structure containing a bond with unusually high ellipticity is potentially unstable. From the Table 1 one can see that the ε values for all M–O bonds are rather small and are variable in a narrow range 0.034–0.138 indicating the M–O bonds dynamic stability.

The binding energy value of cation to the TOC-ligand calculated by the DFT-approach is generally correlates with QTAIM predictions. However, the BE value is much higher than the sum of corresponding M–O bonds energies obtained from the QTAIM analysis (Table 2). Such large binding energy differences can be explained by the fact that the solvation energy should be taken into account for the estimation of the dissociation energies at the DFT/B3LYP level like it was demonstrated in ref. 24*d*. In contrast, the estimation of complexation energy by the Bader's algorithm is

Table 2 Bond length (d) and selected topological parameters of the electron density distribution function $\rho(\mathbf{r})$ of the M–O bonds

								E	BE[b]	BE[b]/n	BE[c]	BE[b] + D
Complex	Bond	d, Å	$\rho(\mathbf{r})$, $e \times a_0^{-3}$	$\nu(\mathbf{r})$, au	$g(\mathbf{r})$, au	$h_e(\mathbf{r})$[a], au	$\nabla^2\rho(\mathbf{r})$, $e \times a_0^{-5}$	kcal mol^{-1}				
1	$Li^+\cdots O$	2.040	2.03×10^{-2}	-2.08×10^{-2}	2.80×10^{-2}	0.12×10^{-2}	0.140	−6.5	−91.5	−22.9	−95.7	−94.8
2	$Mg^{2+}\cdots O$	2.036	3.85×10^{-2}	-4.90×10^{-2}	6.04×10^{-2}	1.15×10^{-2}	0.288	−15.4	−289.8	−72.5	−294.5	−293.3
3	$K^+\cdots O$	2.983	9.28×10^{-3}	-7.15×10^{-3}	8.51×10^{-3}	1.36×10^{-3}	3.95×10^{-2}	−2.2	−47.3	−11.8	−52.0	−50.7
4	$Sr^{2+}\cdots O$	2.954	1.25×10^{-2}	-7.89×10^{-3}	1.02×10^{-2}	2.34×10^{-3}	5.03×10^{-2}	−2.5	−48.7	−12.2	−53.6	−52.3
5	$Ba^{2+}\cdots O$	2.976	1.77×10^{-2}	-1.26×10^{-2}	1.33×10^{-2}	0.74×10^{-3}	5.63×10^{-2}	−4.0	−59.9	−15.0	−65.7	−63.7
6	$K^+\cdots O$	2.853	1.21×10^{-2}	-9.92×10^{-3}	1.15×10^{-2}	1.58×10^{-3}	5.23×10^{-2}	−3.1	−108.2	−13.5	−113.2	−113.1
7	$Ca^{2+}\cdots O$	2.622	1.95×10^{-2}	-1.77×10^{-2}	2.00×10^{-2}	2.34×10^{-3}	8.94×10^{-2}	−5.5	−173.4	−21.7	−178.7	−178.5

[a] $h_e(\mathbf{r}) = \nu(\mathbf{r}) + g(\mathbf{r})$, where $g(\mathbf{r})$ is the kinetic energy density at the (3, −1) critical point; $1/4\nabla^2\rho(\mathbf{r}) = 2g(\mathbf{r}) + \nu(\mathbf{r})$. [b] BSSE corrected. [c] BSSE uncorrected binding energy of cation to the TOC-ligand at 0 K calculated by the DFT/B3LYP approach in a gas phase without zero-point energy (ZPE) correction; D – the dispersion correction upon complexation for the studied **1–7** species calculated by the DFT/B3LYP + D approach; n is the number of the equivalent coordination M–O bonds ($n = 4$ for complexes **1–5** and $n = 8$ for **6** and **7**).

based on the calculation of the potential energy density at the corresponding (3, −1) bond critical point. In this case solvation energy has a minimal contribution, because of $\nu(\mathbf{r})$ values slightly depend on solvation effect.

We should note, that the BE values are comparable well with the same values for the complexes of the alkali and alkaline-earth metals with the classical crown ethers calculated by the DFT-approach in the gas phase.[24d,e] For example, the binding energy of Mg^{2+} ion is much larger than that for other cations, which is quantitatively agreed with the binding energy of Mg^{2+} with classical dibenzo-18-crown-6-ether.[24d]

3. QTAIM analysis of M–O interactions in the two-decker sandwich-type complexes 6, 7

As we have discussed before, some ions (which size is higher than the corresponding crown cavity) are able to sit at the top of the cavity forming the M–O coordination bonds. However we have not obtained the stable s-block metal complexes with the single-TOC ligand. Whereas the double-TOC ligands seem to be able to form the sandwich complexes with some cations. We have obtained two stable sandwiches consisting of the Ca^{2+} and K^+ central ions (Fig. 3). The K^+–O and Ca^{2+}–O bonds occurring in the double-decker complexes **6** and **7** (Fig. 3) are characterized by the following conditions: $|\lambda_1/\lambda_3| < 1$ and $\nabla^2\rho(\mathbf{r}) > 0$, $h_e(\mathbf{r}) > 0$, which correspond to the closed shells interactions similar to the single-decker complexes. The DI value is much smaller for the K^+–O bond than for the Ca^{2+}–O bond which is determined by the stronger polarization affinity of the double-charged Ca^{2+} ion relative to oxygen atoms comparing with the single-charged K^+ ion (Table 1).

As one can see from Fig. 3, the K^+ and Ca^{2+} cations are symmetrically held between the two TOC planes by the "sandwich" principle due to formation of eight equivalent M–O bonds with energies −3.1 and −5.5 kcal mol^{-1}, respectively (Table 2). The QTAIM analysis has also predicted an additional stabilization of the complexes **6** and **7** due to the presence of π-stacking C···C interactions between two TOC parallel plains. The total energy of these inter-plain π-stacking contacts calculated by the eqn (1) equals to 2.2 and 12.6 kcal mol^{-1} for **6** and **7** complexes, respectively (Fig. 3). Such large energy difference can be explained by the shorter inter-plain distance (between the TOC sheets) for the complex **7** than for the complex **6** (b = 3.945 for complex **6**, whereas b = 3.254 Å for complex **7**, Fig. 3). As a result, a greater accumulation of the local potential energy density has observed in the inter-plane space of the complex **6** comparing with the complex **7**. As a conclusion remark we should note that the both TOC sheets are planar in the unbound state but they are definitely bent upon the complexation with the metal ions (Fig. 3b) due to the M–O and π-stacking bonds occurrence (bend angle estimated as 4° and 6° for the complexes **6** and **7**).

Conclusions

On the ground of the DFT calculations the highly symmetrical s-block metal complexes with the tetraoxa[8]circulene sheet ligands have been designed and the Bader's QTAIM analysis have been carried out for their optimized structures. We have proposed the two different types of complexes (square-planar and two-decker sandwich types) consisting of the TOC ligands with the different size cavities (small 16-crown-4 one and the bigger 20-crown-4 cavity). In fact, we have observed the definite selectivity of the ion complexation depending on a strict correlation between the cavity size and cation radii (similar to the "key-lock" principle). This observation should be useful for the creation of the TOC-based nanosheets representing the promising synthetic ionic channels like the already known biomimetic graphene nanopores.[11d] Moreover, the disk-like TOC-based sheets can find potential applications in bio-analytical chemistry due to their interesting DNA recognition properties.[25]

Concerning the general structural features of the designed complexes we should note that the mutual polarization of the alkali or alkaline-earth metal cations and of the organic tetradentate TOC ligand leads to the relatively low accumulation of electron density in the M–O bonds inter-atomic space. As a result, all these M–O bonds have been classified as the closed shell interactions, *i.e.* ionic bonds possess the small covalent character. The last parameter has been estimated on the basis of the electron density delocalization indices being relatively small in comparison with the most of coordination bonds. All studied complexes demonstrate the high symmetry of the coordination sphere: these are square-shaped for the single-decker planar complexes and a proper prism-shaped form for the double-decker complexes both types being correspond to the D_{4h} symmetry point group.

Acknowledgements

All the computations were performed with the resources provided by the Swedish National Infrastructure for Computing (SNIC) at the Parallel Computer Center (PDC) through the project "Multiphysics Modeling of Molecular Materials", SNIC 020/11-23. This research was also supported by the Ministry of Education and Science of Ukraine (project number 0113U001694).

Notes and references

1 (*a*) C. J. Pedersen, *J. Am. Chem. Soc.*, 1967, **89**, 2495–2496; (*b*) C. J. Pedersen, *J. Am. Chem. Soc.*, 1967, **89**, 7017–7036; (*c*) C. J. Pedersen, *J. Am. Chem. Soc.*, 1970, **92**, 386–391; (*d*) C. J. Pedersen, *J. Am. Chem. Soc.*, 1970, **92**, 391–394; (*e*) C. J. Pedersen, *J. Org. Chem.*, 1971, **36**, 254–257; (*f*) C. J. Pedersen, *J. Org. Chem.*, 1971, **36**, 1690–1693.

2 (*a*) D. P. Zollinger, E. Bulten, A. Christenhusz, M. Bos and W. E. Van Der Linden, *Anal. Chim. Acta*, 1987, **198**, 207–222; (*b*) R. M. Izalt, K. Pawlak and J. S. Bradshaw, *Chem. Rev.*, 1991, **91**, 1721–2085; (*c*) P. S. H. Wong, B. J. Antonio and D. V. Dearden, *J. Am. Soc. Mass Spectrom.*, 1994, **5**, 632–637; (*d*) A. Datta, *J. Phys. Chem. C*, 2009, **113**, 3339–3344.

3 (*a*) E. B. Fleischer, *Acc. Chem. Res.*, 1970, **3**, 105–112; (*b*) B. Minaev, *Spectrochim. Acta, Part A*, 2004, **60**, 3213–3224;

(*c*) B. Minaev and H. Agren, *Chem. Phys.*, 2005, **315**, 215–239; (*d*) M. G. Waltera, A. B. Rudineb and C. C. Wamser, *J. Porphyrins Phthalocyanines*, 2010, **14**, 759–792.

4 A. B. P. Lever, *Adv. Inorg. Chem. Radiochem.*, 1965, **7**, 27–114.

5 (*a*) V. Balzani and A. Juris, *Coord. Chem. Rev.*, 2001, **211**, 97–115; (*b*) R. McGuire Jr, M. C. McGuireb and D. R. McMillinb, *Coord. Chem. Rev.*, 2010, **254**, 2574–2583; (*c*) Y.-W. Zhong, C.-J. Yao and H.-J. Nie, *Coord. Chem. Rev.*, 2013, **257**, 1357–1372.

6 M. Chastrette and F. Chastrette, *J. Chem. Soc., Chem. Commun.*, 1973, 534–535.

7 Y. Kobuke, K. Hanji, K. Horiguchi, M. Asada, Y. Nakayama and J. Furukawa, *J. Am. Chem. Soc.*, 1976, **98**, 7415–7419.

8 (*a*) Z. Shi and N. Lin, *J. Am. Chem. Soc.*, 2010, **132**, 10756–10761; (*b*) S. Banala, R. G. Huber, T. Müller, M. Fechtel, K. R. Liedl and B. Kräutler, *Chem. Commun.*, 2012, **48**, 4359–4361; (*c*) S. Banala, K. Wurst and B. Kräutler, *J. Porphyrins Phthalocyanines*, 2014, **18**, 116–122; (*d*) Y. Li, J. Xiao, T. E. Shubina, M. Chen, Z. Shi, M. Schmid, H.-P. Steinruck, J. M. Gottfried and N. Lin, *J. Am. Chem. Soc.*, 2012, **134**, 6401–6408.

9 (*a*) H. Erdtman and H.-E. Högberg, *Chem. Commun.*, 1968, 773; (*b*) H. Erdtman and H.-E. Högberg, *Tetrahedron Lett.*, 1970, **11**, 3389; (*c*) H.-E. Högberg, *Acta Chem. Scand.*, 1972, **26**, 309; (*d*) H.-E. Högberg, *Acta Chem. Scand.*, 1972, **26**, 2752; (*e*) H.-E. Högberg, *Acta Chem. Scand.*, 1973, **27**, 2559; (*f*) H.-E. Högberg, *Acta Chem. Scand.*, 1973, **27**, 2591; (*g*) J. Eskildsen, T. Reenberg and J. B. Christensen, *Eur. J. Org. Chem.*, 2000, 1637; (*h*) C. B. Nielsen, T. Brock-Nannestad, T. K. Reenberg, P. Hammershoj, J. B. Christensen, J. W. Stouwdam and M. Pittelkow, *Chem.–Eur. J.*, 2010, **16**, 13030; (*i*) A. Datta and S. K. Pati, *J. Phys. Chem. C*, 2007, **111**, 4487–4490.

10 (*a*) B. F. Minaev, G. V. Baryshnikov and V. A. Minaeva, *Comput. Theor. Chem.*, 2011, **972**, 68; (*b*) A. Minaeva, B. F. Minaev, G. V. Baryshnikov, H. Agren and M. Pittelkow, *Vib. Spectrosc.*, 2012, **61**, 156; (*c*) G. V. Baryshnikov, B. F. Minaev, M. Pittelkow, C. B. Nielsen and R. Salcedo, *J. Mol. Model.*, 2013, **19**, 847; (*d*) N. N. Karaush, B. F. Minaev, G. V. Baryshnikov and V. A. Minaeva, *Opt. Spectrosc.*, 2014, **116**, 33–46; (*e*) G. V. Baryshnikov, R. R. Valiev, N. N. Karaush and B. F. Minaev, *Phys. Chem. Chem. Phys.*, 2014, **16**, 15367–15374; (*f*) G. V. Baryshnikov, B. F. Minaev, N. N. Karaush and V. A. Minaeva, *Phys. Chem. Chem. Phys.*, 2014, **16**, 6555–6559; (*g*) G. V. Baryshnikov, B. F. Minaev, N. N. Karaush and V. A. Minaeva, *RSC Adv.*, 2014, **4**, 25843–25851; (*h*) J. Yu, Q. Sun, Y. Kawazoe and P. Jena, *Nanoscale*, 2014, **6**, 14962–14970.

11 (*a*) J. Luo, X. Xu, R. Mao and Q. Miao, *J. Am. Chem. Soc.*, 2012, **134**, 13796–13803; (*b*) K. Nakanishi, D. Fukatsu, K. Takaishi, T. Tsuji, K. Uenaka, K. Kuramochi, T. Kawabata and K. Tsubaki, *J. Am. Chem. Soc.*, 2014, **136**, 7101–7109; (*c*) M. J. Ackerman and D. E. Clapham, *N. Engl. J. Med.*, 1997, **336**, 1575–1586; (*d*) Y. Kang, Z. Zhang, H. Shi, J. Zhang, L. Liang, Q. Wang, H. Agren and Y. Tu, *Nanoscale*, 2014, **6**, 10666–10672.

12 (*a*) Y. Nakamura, N. Aratani, K. Furukawa and A. Osuka, *Tetrahedron*, 2008, **64**, 11433–11439; (*b*) Y. Nakamura, N. Aratani, H. Shinokubo, A. Takagi, T. Kawai, T. Matsumoto, Z. S. Yoon, D. Y. Kim, T. K. Ahn, D. Kim, A. Muranaka, N. Kobayashi and A. Osuka, *J. Am. Chem. Soc.*, 2006, **128**, 4119–4127.

13 (*a*) V. E. Pushkarev, E. V. Shulishov, Y. V. Tomilov and L. G. Tomilova, *Tetrahedron Lett.*, 2007, **48**, 5269–5273; (*b*) S. Alpugan, Ü. Işci, F. Albrieux, C. Hirel, A. G. Gürek, Y. Bretonniére, V. Ahşena and F. Dumoulin, *Chem. Commun.*, 2014, **50**, 7466–7468.

14 (*a*) R. F. W. Bader, *Atoms in Molecules. A Quantum Theory*, Calendon Press, Oxford, 1990; (*b*) R. F. W. Bader and H. Essen, *J. Chem. Phys.*, 1984, **80**, 1943–1960; (*c*) R. F. W. Bader, T. S. Slee, D. Cremer and E. Kraka, *J. Am. Chem. Soc.*, 1983, **105**, 5061–5068; (*d*) C. L. Firme, O. A. C. Antunes and P. M. Esteves, *Chem. Phys. Lett.*, 2009, **468**, 129–133.

15 J. D. Lee, *Concise Inorganic Chemistry*, Chapman & Hall, New York, 1991.

16 (*a*) A. D. Becke, *J. Chem. Phys.*, 1993, **98**, 5648–5652; (*b*) C. Lee, W. Yang and R. G. Parr, *Phys. Rev. B: Condens. Matter Mater. Phys.*, 1988, **37**, 785–789.

17 (*a*) R. Krishnan, J. S. Binkley, R. Seeger and J. A. Pople, *J. Chem. Phys.*, 1980, **72**, 650–654; (*b*) P. J. Hay and P. J. Wadt, *J. Phys. Chem.*, 1985, **82**, 270–283.

18 (*a*) E. Espinosa, E. Molins and C. Lecomte, *Chem. Phys. Lett.*, 1998, **285**, 170–173; (*b*) E. Espinosa, I. Alkorta and I. Rozas, *Chem. Phys. Lett.*, 2001, **336**, 457–461; (*c*) G. V. Baryshnikov, B. F. Minaev, A. A. Korop, V. A. Minaeva and A. N. Gusev, *Russ. J. Inorg. Chem.*, 2013, **58**, 928–934; (*d*) L. N. Puntus, K. A. Lyssenko, M. Y. Antipin and J.-C. G. Bünzli, *Inorg. Chem.*, 2008, **47**, 11095–11107; (*e*) A. O. Borissova, M. Y. Antipin, H. A. Karapetyan, A. M. Petrosyan and K. A. Lyssenko, *Mendeleev Commun.*, 2010, **20**, 260–262; (*f*) G. V. Baryshnikov, B. F. Minaev, V. A. Minaeva and V. G. Nenajdenko, *J. Mol. Model.*, 2013, **19**, 4511–4519.

19 D. Cremer and E. Kraka, *Croat. Chem. Acta*, 1984, **57**, 1259–1281.

20 F. Neese, *Orca – An Ab Initio, Density Functional and Semiempirical Program Package, Version 2.8*, University of Bonn, Bonn, Germany, 2010.

21 M. J. Frisch, G. W. Trucks, H. B. Schlegel, G. E. Scuseria, M. A. Robb, J. R. Cheeseman, G. Scalmani, V. Barone, B. Mennucci, G. A. Petersson, H. Nakatsuji, M. Caricato, X. Li, H. P. Hratchian, A. F. Izmaylov, J. Bloino, G. Zheng, J. L. Sonnenberg, M. Hada, M. Ehara, K. Toyota, R. Fukuda, J. Hasegawa, M. Ishida, T. Nakajima, Y. Honda, O. Kitao, H. Nakai, T. Vreven, J. A. Montgomery Jr, J. E. Peralta, F. Ogliaro, M. Bearpark, J. J. Heyd, E. Brothers, K. N. Kudin, V. N. Staroverov, R. Kobayashi, J. Normand, K. Raghavachari, A. Rendell, J. C. Burant, S. S. Iyengar, J. Tomasi, M. Cossi, N. Rega, J. M. Millam, M. Klene, J. E. Knox, J. B. Cross, V. Bakken, C. Adamo, J. Jaramillo, R. Gomperts, R. E. Stratmann, O. Yazyev, A. J. Austin, R. Cammi, C. Pomelli, J. W. Ochterski, R. L. Martin, K. Morokuma, V. G. Zakrzewski, G. A. Voth,

P. Salvador, J. J. Dannenberg, S. Dapprich, A. D. Daniels, Ö. Farkas, J. B. Foresman, J. V. Ortiz, J. Cioslowski and D. J. Fox, *Gaussian 09, revision C.02*, Gaussian, Inc., Wallingford, CT, 2009.

22 T. A. Keith, http://www.aim.tkgristmill.com, 2010.

23 R. D. Shannon, *Acta Crystallogr., Sect. A: Cryst. Phys., Diffr., Theor. Gen. Crystallogr.*, 1976, **32**, 751–767.

24 (*a*) M. Monajjemi and J. Najafpour, *Am. J. Res. Commun.*, 2013, **1**, 13–30; (*b*) E. D. Glendening, D. Feller and M. A. Thompson, *J. Am. Chem. Soc.*, 1994, **116**, 10657–10669; (*c*) Y. Inokuchi, O. V. Boyarkin, R. Kusaka, T. Haino, T. Ebata and T. R. Rizzo, *J. Am. Chem. Soc.*, 2011, **133**, 12256–12263; (*d*) J. Heo, *Bull. Korean Chem. Soc.*, 2012, **33**, 2669–2674; (*e*) C. M. Choi, J. Heo and N. J. Kim, *Chem. Cent. J.*, 2012, **6**, 84–91.

25 (*a*) A. K. Jissy and A. Datta, *ChemPhysChem*, 2012, **13**, 4163–4172; (*b*) A. K. Jissy, U. P. M. Ashik and A. Datta, *J. Phys. Chem. C*, 2011, **115**, 12530–12546.